SUPERLATTICES OF ATOMS, MOLECULES AND ISLANDS

H. BRUNE

Institut de Physique des Nanostructures
Ecole Polytechnique Fédérale de Lausanne (EPFL)
CH-1015 Lausanne, Switzerland

Abstract. We describe the state-of-the-art in the creation of ordered superlattices of adsorbed atoms, molecules, semiconductor quantum dots, and metallic islands, by means of self-assembly during atomic-beam growth on single crystal surfaces. These surfaces often have long-period reconstructions or strain relief patterns which are used as template for heterogeneous nucleation. However, repulsive adsorbate-adsorbate interactions may also stabilize ordered superlattices, and vertical correlations of growth sequences of buried islands will be discussed in the case of semiconductor quantum dots. We also present new template surfaces considered as particularly promising for the creation of novel island superlattices.

Keywords:

Contents

1. Introduction

In this chapter we describe several means to create ordered superlattices of adsorbed atoms, molecules, semiconductor quantum dots, and metallic

islands, and finally we describe templates which might be used in the future to create novel island superlattices. In most cases the approach is based on kinetically controlled growth by means of molecular beam epitaxy (MBE) onto a low-index single crystal surface. The creation of order is based on the hierarchy of activation energies of the atomic and molecular displacements, and on the variation of the binding energy as a function of lateral position on the surface, inducing a directional variation in the diffusion barriers and thereby a diffusion current directed to particular surface sites. In a few cases kinetically controlled growth can be followed by gentle annealing enabling the formation of energetically favored structures or sizes, so-called magic islands.

The interest in growing large ensembles of nanostructures with well-defined sizes is the investigation of their physical and chemical properties as a function of size and composition, ideally in an atom-by-atom, or molecule-by-molecule way. Many properties can so far only be investigated with spatially integrating techniques, requiring high densities of uniform particles. As an example, the methods presented here have already unravelled the spectacular increase of the orbital magnetic moment and magnetic anisotropy energy of Co islands on Pt(111) with decreasing size [1]. A second aim of creating molecular, atomic, or island superlattices is to study the properties specific of the ensemble, i.e., the properties emerging from their mutual interactions. One example is a superlattice of Kondo scatterers [2,3], or dipolar interactions between magnetic particles [4].

At first glance the attempt to create long-range ordered periodic and almost monodisperse structures seems impossible due to the statistics in time and space inherent in deposition and in the Brownian motion of the adsorbed species. On homogeneous substrates this leads to interdependent spatial and size distributions of the islands with width and shape given by well-known scaling laws of nucleation [5–8]. In the temperature regime where dimers are stable on the time scale of deposition, the half-width at half-maximum (HWHM) of the size distribution is 0.55 times the average size, which is rather polydisperse. We shall show below that heterogeneous nucleation on equidistant sites leads to much better results and therefore, to some extent, one may create order out of randomness.

We first discuss atomic and molecular superlattices which are stabilized by repulsive interactions due to electronic screening in a two-dimensional (2D) electron gas of a surface state. In this case the perfect lattice distance represents a shallow minimum in total energy. Diffusion has to be activated to reach this minimum; however, it also creates Brownian motion

and a liquid-like-state, such that the degree of order depends on the ratio between interaction energy and diffusion barrier. Our second example will be strain-mediated vertical stacking of buried semiconductor quantum dots. The spacer layers covering the quantum dots are inhomogeneously strained leading to correlations in the nucleation of the quantum dots grown on-top. With an increasing amount of quantum dot and spacer layers, the order is increased since the strain fields of too close dots coalesce, and randomness leads to nucleation of new dots between two dots which are too far apart. The best size distributions have a HWHM of 0.08, and the dot distance can to some extent be tuned by the thickness of the spacer layers. Then we turn our attention back to two-dimensional systems where elastic interactions mediated by the substrate lead to mesoscopically periodic surfaces. Such surfaces represent long-range modulated potential energy surfaces for deposited species to which their periodic structure may be transferred. The focus is on recent work and the reader is referred to the literature for former work on the nucleation on strain relief patterns [9]. We close by showing a few template surfaces which have been discovered very recently and have not yet been employed as templates for the growth of ordered superlattices.

2. Stabilization of Superlattices by Friedel Oscillations in Surface States

An impurity atom in a solid induces a variation in the potential acting on the host conduction electrons, which they screen by oscillations in their density. Friedel introduced such oscillations with wave vector $2k_{\mathrm{F}}$ to calculate the conductivity of dilute metallic alloys [10]. In addition to the pronounced effect on the relaxation time of conduction electrons, Friedel oscillations may also be a source of mutual interactions between impurity atoms through the fact that the binding energy of one such atom in the solid depends on the electron density into which it is embedded, and this quantity oscillates around another impurity atom. Lau and Kohn predicted such interactions to depend on distance as $\cos(2k_{\mathrm{F}}r)/r^5$ [11]. We note that for isotropic Fermi surfaces there is a single k_{F}-value, whereas in the general case one has to insert the Fermi vector pointing into the direction of the interaction [12,13]. The electronic interactions are oscillatory, and their $1/r^5$-decay is steeper than the monotonic $1/r^3$-decay of elastic interactions [14]. Therefore elastic interactions between bulk impurities dominate the electronic ones from relatively short distances on.

This situation is quite different in 2D. The pair interaction energy between two impurities caused by screening in a 2D electron gas was predicted to be proportional to $\cos(2k_{\mathrm{F}}r)/r^2$ [11]. This relatively slow decay implies that electron mediated interactions in 2D dominate elastic and dipolar ones, giving rise to interactions between impurities which oscillate between attraction and repulsion as a function of distance. The first experimental observation indicative of long-range interactions, possibly mediated by 2D Friedel oscillations, came from equidistant bulk segregated impurities on Cu(111) [15]. However, the quantitative determination of the interaction energy as a function of distance became possible only very recently [16,17].

The required 2D nearly free electron gas is realized in Shockley type surface states of close-packed surfaces of noble metals. These states are located in narrow band gaps in the center of the first Brillouin zone of the (111)-projected bulk band structure. The fact that their occupied bands are entirely in bulk band gaps separates the electrons in the 2D surface state from those in the underlying bulk. Only at structural defects, such as steps or adsorbates, is there an overlap of the wave functions, opening a finite transmission between the 2D and the 3D system. The fact that the surface state band is narrow implies extremely small Fermi wave vectors and consequently the Friedel oscillations of the surface state have a significantly larger wave length than those of bulk states.

Scanning tunneling microscopy (STM) images taken at low bias directly reflect the oscillating quantity, namely the LDOS close to E_{F}, thus enabling direct observation of Friedel oscillations [18]. Figure 1(a) shows Friedel oscillations on Ag(111) which has a surface state with $k_{\mathrm{F,surf}} = 0.083\,\text{Å}^{-1}$ [19] (compare $k_{\mathrm{F,bulk}} = 1.2\,\text{Å}^{-1}$ [20]). There are two substitutional defects appearing as protrusions on the otherwise clean surface. They induce a smooth modulation in the apparent height of the Ag atoms extending over the entire image. These are the surface state Friedel oscillations [21] which are readily detectable up to more than 100 Å distance in the large scale STM image Fig. 1(b).

Figure 1(c) shows Friedel oscillations around Cu atoms adsorbed onto a Cu(111) surface, which equally has a surface state ($k_{\mathrm{F}} = 0.21\,\text{Å}^{-1}$ [21]). The STM image is taken out of a sequence of images recorded at 13.5 K where Cu adatoms readily diffuse (for videos see the author's website under gallery). Despite the fact that the atoms quite often come close to each other, they do not form islands but remain isolated during the observation time of several hours. This is remarkable for a metallic system and can only be reconciled by a significant short-range repulsion. For the present

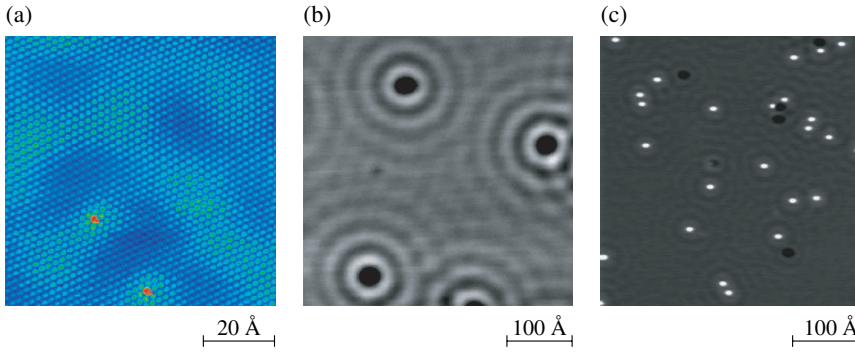

Fig. 1. (a) Two substitutional defects on Ag(111) ($V_t = -5\,\mathrm{mV}, I_t = 8\,\mathrm{nA}, T = 9\,\mathrm{K}$). (b) Large view of (a) showing the long-range oscillations with $\lambda = \pi/k_F = 38\,\text{Å}$ around 4 point defects on Ag(111) ($V_t = 24\,\mathrm{mV}$, $I_t = 0.5\,\mathrm{nA}$, $T = 9\,\mathrm{K}$). (c) Still from time sequence of STM images recorded to trace diffusing Cu atoms on Cu(111) (coverage $\Theta = 1.4 \times 10^{-3}\,\mathrm{ML}$, 1 ML is defined by one adatom per atom of the substrate surface, $V_t = 100\,\mathrm{mV}$, $I_t = 0.5\,\mathrm{nA}$, $T = 13.5\,\mathrm{K}$). From [17].

system, no cluster formation was observed during annealing at 16.5 K for 20 min. On the other hand, almost all the monomers formed islands during annealing at 22 K for a comparable time. From these observations the short-range repulsion has been estimated to be between 10 and 14 meV [22]. This energy can only partly be caused by surface state Friedel oscillations. Its main origins are more likely dipole-dipole, elastic, or bulk-electron mediated interactions. Such short-range interactions have been studied by means of field ion microscopy (FIM) [23] and STM [24,25]. We note here that their existence is mandatory for the observation of the long range interactions we are after, since they stabilize the adatom gas and prevent nucleation.

Inspection of Fig. 1(c) reveals that there are a few pairs of atoms with a preferred distance. Analysis of many such images in terms of site occupation probabilities as a function of adatom distances revealed significant deviations from a random distance distribution, and the existence of adsorbate interactions which indeed oscillated with a wave vector of $2k_F$ [16]. The decay followed the $1/r^2$-prediction only for large distances, while significant deviations were observed at distances below 20 Å and interpreted as a shortcoming of theory [16]. However, an independent study, carried out in parallel, focused on two body interactions only, i.e., the authors counted only those distances r from a selected atom to a nearby atom where no third scatterer (adatom or impurity) was closer than r [17]. This way, many body interactions were eliminated and the interaction energy $E(r)$ yielded perfect

agreement with the theoretically predicted decay down to 5 Å distance. The energy was of the form $E(r) = -AE_0(2\sin\delta\pi)^2\sin(2qr+2\delta)/((qr)^2+(qc)^2)$, with A the scattering amplitude, δ the scattering phase [26], and c a fit parameter. The wave vectors q were found to be in perfect agreement with the Fermi-vectors of the respective host surface states, for Co atoms diffusing and interacting on Ag(111), and for Co and Cu atoms on Cu(111) [17]. The theoretically predicted oscillatory long-range interactions between adsorbates were experimentally confirmed.

Note, however, that the interaction energy is very small; for example the depth of the first energy minimum in the pair potential of Cu/Cu(111) amounts only to 2 meV [17]. This energy is small compared to the diffusion barrier of 40 ± 1 meV [17] implying first that the atoms always reside on surface lattice sites, and second that high temperatures are needed to reach the shallow minimum. Too high temperatures, on the other hand, lead to irreversible nucleation due to the limited short range repulsion of 12 ± 2 meV, thus determining a narrow temperature window for the pair interactions to be studied. Early attempts to use these interactions for the formation of atomic superlattices failed [16,17]. Figure 2(a) shows the case of Cu/Cu(111) where chains of equidistant atoms are formed but there are only small patches of hexagonally close packed atomic superlattices. This was also the case for Co on the same substrate, whereas Co/Ag(111) showed quasi hexagonal lattices, which were, however, not well-ordered [17]. The breakthrough came for the system Ce/Ag(111) where the Ce atoms are forming well-ordered hexagonal superlattices with a lattice constant of 32 Å,

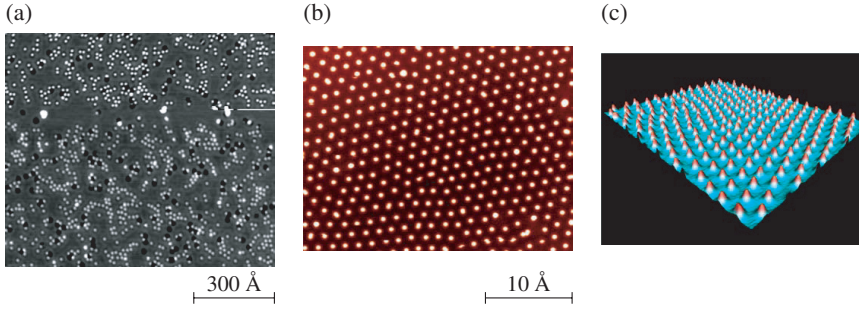

Fig. 2. (a) For Cu/Cu(111) the surface state mediated long-range interactions favor atomic chains with inter-atomic distances of 12 Å, but not hexagonal lattices ($\Theta = 6\times10^{-3}$ ML, $T = 15$ K, $V_t = -0.3$ V and $I_t = 2.0$ nA). (b) and (c) STM images of well-ordered Ce superlattices formed on Ag(111) ($\Theta = 8\times10^{-3}$ ML, $T = 3.9$ K, $V_t = 0.1$ V and $I_t = 10$ pA). Figures (b) and (c) are kindly provided by W. D. Schneider.

see Figs. 2(b) and (c) [2]. Note that Ce atoms on Ag(111) are Kondo scatterers, thus Fig. 2(c) shows a superlattice of Kondo impurities which may interact also electronically via the 2D surface state electron gas [2,3]. The dilute atomic superlattices are most nicely ordered at 3.9 K, whereas the atoms start to diffuse around their ideal positions at 4.8 K, corresponding to a 2D dilute liquid, and the lattice is destroyed by irreversible nucleation of Ce islands at 10 K.

The question why superlattices could be formed for Ce/Ag(111) and not for the other systems studied before is at present not fully settled. Let us point out a few differences between the systems and discuss their possible consequences. For Ce/Ag(111), the first minimum in the pair potential is 0.8 meV deep and the diffusion barrier 12 meV, therefore the relative strength of the long-range interaction is slightly larger (1/15) than for Cu/Cu(111) (1/20). The relative stability toward irreversible nucleation is also slightly larger for Ce/Ag (10 K/12 meV vs. 22 K/40 meV). This enables one to reach higher relative temperatures bringing the system closer to the total energy minimum. Note, however, that temperature also creates disorder; in the case of Ce/Ag one can even melt the dilute solid before it collapses into an island. A third item favoring Ce/Ag over Cu/Cu is its scattering phase of $\delta = (0.37 \pm 0.05)\pi$ vs. $\delta = (0.50 \pm 0.07)\pi$. The phase determines the position of the first interaction maximum and thereby the surface area around an adatom in which deposited atoms become irreversibly attached to the adatom. This area is smaller when the phase is smaller, favoring Ce/Ag. A second order effect of the phase is to determine whether the $\sqrt{3}$ distance appearing as second neighbor distance in hexagonal lattices is favored.

The arguments above are for pair interactions. Once a germ of a hexagonal lattice is formed, these interactions add up and lead in the case of Ce/Ag to an energy minimum of (4.9 ± 0.5) meV for a six-fold coordinated Ce atom, and to a repulsion of (11.8 ± 1.2) meV when it approaches one of its six neighbors [2]. These energies compare favorably with the diffusion barrier and suggest that having used higher coverages may well have helped to create superlattices as well for Cu or Co/Cu(111). For Co/Ag(111) the interaction was comparable to Ce, and also the scattering phase; however, the diffusion barrier was much larger (in the range of 50 meV [27]).

Let us discuss a few more consequences of the fact that repulsive adsorbate-adsorbate interactions add up. The formation of superlattices may be hampered by adding up interactions since this may favor attachment to the ends of elongated structures compared to their sides. In the

extreme case, this leads to the formation of straight 1D chains, as was first observed by means of FIM for interactions of intermediate range [28]. Ir atoms were reported to diffuse at some distance along Ir chains on W(110), and attach exclusively to their ends. Calculations for Ag on compressively strained Ag(111) and Cu/Cu(111) reported strongly anisotropic repulsive barriers around elongated islands (dimers, linear trimers) favoring attachment to their ends [29]. A similar phenomenon has been reported to hold also for the long-range interactions. For Co/Cu(111) the individual interactions were shown to add up leading to an attachment barrier of 22 meV for atoms approaching from the side to a chain of Co atoms sitting on the distance favored by the interations, whereas there was no attachment barrier to the chain ends [30]. This is in agreement with the preference for linear structures over compact ones observed in experiment for Cu and Co on Cu(111) [17]. However, the precise role of the scattering phase and of multiple interactions in the formation of superlattices is not yet settled and would be worth further exploration. A particular promising way are *ab initio* calculations of long-range interactions fed into kinetic Monte-Carlo (KMC) simulations. Recent calculations of the long-range interactions of 3*d* elements on Cu(111) will stimulate experiments since they predict particular superlattice stability for a number of elements, most spectacularly for Ti [31]. Calculating the diffusion barriers for these systems could enable KMC simulations of the kinetics of superlattice formation and stability.

A further consequence of intermediate-range interactions adding up are very high almost isotropic repulsive barriers around compact clusters. This has consequences for the density scaling [32] and favors small islands with more narrow distributions of sizes and spacings than the ones obtained without interactions [29]. We finally note that atomic superlattices with smaller lattice constant may be stabilized by dipolar interactions of relatively short range. The most prominent examples for such interactions are alkali metals on metal surfaces. A phase transition from a dilute liquid into a well-ordered solid has been reported for Cs/Ag/Si(111)-($\sqrt{3} \times \sqrt{3}$) [33].

The example of Ce/Ag demonstrates that the surface state electron mediated adsorbate-adsorbate interactions may well be employed for the creation of ordered atomic and possibly also molecular superlattices. In principle the lattice constant can be adjusted by the surface state band structure.

3. Order in Vertically Stacked Quantum Dots

There is considerable effort to create 2D and 3D superlattices of semiconductor quantum dots (QDs). This interest is driven by the desire of size uniformity leading to uniform electronic properties evolving from quantum confinement, such as sharp photoluminescence peaks [34]. One of the anticipated applications are quantum dot lasers which have lower threshold currents through the confinement of the current into the active material and are expected to have higher band width. Alternatively to sequential processing techniques involving high-resolution lithography and etching, the spontaneous formation of 3D coherent islands in the Stranski–Krastanow growth mode of lattice-mismatched heteroepitaxial layers has evolved as a novel approach for quantum dot fabrication [35,36]. The formation of 3D islands on-top a wetting layer is driven by the fact that islands allow for an efficient relaxation of elastic energy through their lateral expansion or compression. Because of the statistical nature of growth, these self-assembled dots are usually not very uniform in size, shape, and spacing.

The size uniformity can be improved by growing superlattices with uniform spacings since the distribution of spacings is correlated to the one of sizes [8,39]. A successful way to create such lattices consists of strain-mediated nucleation on-top of islands buried by a spacer layer. Figure 3(a) shows an atomic force microscope (AFM) image of the uppermost uncapped island layer of a growth sequence of Si_xGe_{1-x} quantum dots separated by Si(100) spacer layers burying the QDs. Ge has a 4.2% larger lattice constant than Si, thus the Si spacer is strained to a slightly larger lattice constant on-top of a buried quantum dot, whereas it has its intrinsic lattice constant in-between. The nucleation rate of islands is an exponential function of the nucleation barrier, which depends sensitively on strain [40]. This barrier is lowest where strain in the surface reduces the lattice mismatch between surface and islands. Therefore Si_xGe_{1-x}–alloy islands nucleate preferentially where the Si lattice is expanded, i.e., on-top of a buried island, leading to vertical island correlations in bi-layer stacks. In addition, the following error correction scheme is operative. If by statistical fluctuations two dots are too far apart, there will be a high probability of nucleating one in-between; if two buried dots are too close the strain fields in the Si spacer overlap and only one new QD nucleates on-top, see Fig. 3(b). Repetition of the growth sequence of quantum dots and spacer layer 20 times yields to increased order, as evidenced by Fig. 3(a) [37].

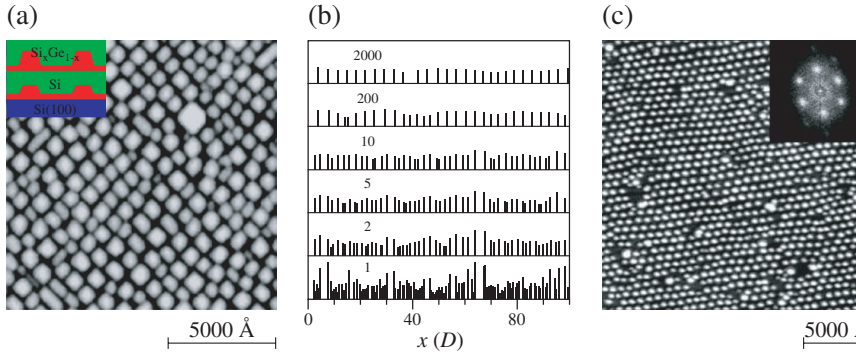

Fig. 3. (a) Ordered arrays of $Si_{0.25}Ge_{0.75}$ quantum dots on Si(100) produced by 20 sequences of Stranski–Krastanov growth of dots and subsequent capping with Si spacer layers (spacer thickness $D = 100$ Å, $Si_{0.25}Ge_{0.75}$ coverage 25 Å). (b) One-dimensional model showing the creation of order by strain fields inducing nucleation on-top of the buried QDs in such a way that statistical variations in QD spacings and sizes (heights of vertical lines) are corrected (distances are given in units of the spacer thickness D, number of growth sequences increases from bottom to top panels as indicated). (c) AFM image of the last PbSe layer of a 60-period $PbSe/Pb_{1-x}Eu_xTe$ dot superlattice grown on PbTe(111) ($x = 5 - 10\%$, PbSe coverage 5 ML, $D = 450$ Å, 360°C growth temperature). The inset shows the 2D power spectrum of the AFM image. (a) and (b) from [37], (c) from [38].

In our example the HWHM of the distribution of island diameters goes from $\sigma = 55\%$ for the first island layer down to $\sigma = 15\%$ after 20 growth sequences [41]. For different material systems, different types of island correlations have been observed, ranging from vertically aligned dot columns for InAs/GaAs [42–44] and SiGe/Si superlattices [37,41], to trigonal dot lattices with fcc stacking for IV–VI superlattices [38]. The lateral island spacing L can be tuned to some extent by the spacer thickness D. There is a linear relationship between the two and the slope depends on the misfit and on the elastic constants. In the model one finds a slope of 3.5, whereas it is larger in the SiGe/Si experiments, and lower for IV–VI superlattices.

Order gets better with increasing the number of QD-spacer sequences. The theoretical model in Fig. 3(b) predicts a monotonic increase of order with increasing bi-layer number, though with decreasing slope. It predicts that one may reach $\sigma = 5\%$ in island volumes after 2000 stacking sequences [37]. For spherical islands this corresponds to $\sigma = 1.7\%$ in diameter (with $V = 4\pi/3\, r^3$ one finds $dV/V = 3\, dr/r$). However, the stress accumulated with increasing number of bi-layers sets an upper limit to the number of stacking sequences on which misfit dislocations normally

start to form. Figure 3(c) shows an example of an entirely strain symmetrized superlattice overcoming this limitation [38,45,46]. This is achieved by adjusting the spacer composition (here $Pb_{1-x}Eu_xTe$) to exactly compensate the tensile stress in the Stranski–Krastanov QD layers (here PbSe). This allows for up to 100 stacking sequences resulting in for semiconductor QDs unprecedented uniformity of $\sigma = 6\%$ in island spacing and $\sigma = 10\%$ in height [38,45]. In the present case the dots are arranged in an fcc-like vertical stacking sequence, due to the (111) growth direction and to the high elastic anisotropy of the material. We note that this system can be grown also with QD correlations parallel to the growth direction by reducing the spacer thickness [46], however, the increase of order with increasing number of stacks is better for the fcc stacking.

The buried QDs form a 3D crystal where the lattice constant can be tuned continuously over several tens of nanometers by the thickness of the spacers, and the size and spacing uniformities increase with number of stacking sequences. For the size uniformity it is essential to distinguish diameter, area, and volume since they typically differ by factors of 2, respectively, 3. Some physical properties may depend on volume, some on area, and some on diameter, thus reflecting the polydispersity in a different way. For instance, the quantization energies are dominated by the smallest dimension of the QDs, which is the height in the cases discussed above.

4. Decorating Mesoscopically Ordered Surface Reconstructions

Surface reconstructions can have large unit cells of up to 25 atoms in length. In addition, the reconstruction may have rotational domains which may be ordered on an even larger length scale into mesoscopic periodic patterns. These surfaces can be used as templates for the heterogeneous nucleation of island superlattices, or for the regular arrangement of single molecules or molecular clusters. One example of mesoscopic order is the herringbone pattern of the Au(111)-($\sqrt{3} \times 22$)-reconstruction [47]. Other examples of relatively long-range 2D periodic surfaces are Au(111)-vicinal surfaces. When miscut towards the $[\bar{2}11]$-azimut, these surfaces present the energetically favored {111}-faceted steps. For a limited range of miscut angles [48] this makes them stable against faceting, and elastic step repulsions give rise to regularly spaced steps [49]. Thus the step distance is solely given by the miscut angle (35 Å on Au(788) and 50 Å on Au(11,12,12)), while the surface period parallel to the steps is caused by the reconstruction of

the (111)-terraces and fixed to about 70 Å. The advantage of vicinals with respect to low-index surfaces is that the superlattice is not perturbed by the steps, and thus phase-coherent over the entire crystal. The Si(111)-(7×7)-reconstruction [50] and the (15×15)-termination of the reduced $Fe_3O_4(111)$ surface [51] are examples of large period semiconductor and oxide surface reconstructions, respectively.

The surfaces mentioned so far have a long-range periodicity in their pristine state, leaving only limited room for adjustment of period, or symmetry. This is different in periodic strain relief patterns created in ultrathin single crystalline films on single crystal substrates, where the period of the superlattice can be adjusted by the misfit between film and substrate. Such incommensurate adlayers exist for metals on metals [9,52–55], dielectrics on metals [56–62], semiconductors on semiconductors [63,64], metals on semiconductors [65], and finally for adsorbates changing the reconstruction of metal films on metals [66]. In principle, one can achieve a continuous tuning of the superlattice period by growing alloy layers for which the lattice constant can be adjusted linearly through the alloy composition, as described by Vegards law. This has been realized for the surface alloy between Au and Ni on a Ni(111) surface [67]. Depending on the lateral stiffness of the film with respect to the corrugation of the substrate potential, one observes moiré patterns with a smooth transition between different stacking sites, or narrow domain walls, which can also be called partial surface dislocations.

These long-range periodic surfaces have been used with success for the heterogeneous nucleation of ordered island superlattices. They have in common the characteristic that nucleation takes place on predefined periodically arranged sites. Therefore the size distribution is given by the statistics of the deposition, leading to a *binomial distribution* of island volumes with $\sigma = \sqrt{(1-\theta)/\theta}/\sqrt{n}$ with n the area of the superlattice unit cell expressed in atoms, and θ as usual the coverage expressed in monolayers [68]. Note that this can lead to quite narrow size distributions obtained in a single deposition step, e.g. $\sigma = 4\%$ for half a monolayer deposited onto a surface with a (25×25) unit cell! For a more detailed description of these systems we refer to the literature [9,48,69–82], and here focus on one case which emerged recently and which seems to be particularly promising.

Ordered strain relief patterns with a large period are most often formed on hexagonally close-packed surfaces since they have a small corrugation of the substrate potential, and the overlayer is relatively stiff since it is

close-packed. For many reasons one is interested to also create square superlattices of islands, atoms, or molecules. One case where this has been achieved with reasonable success is metal decoration of a Cu(100) surface having been prestructured by nitrogen islands. Figure 4(b) shows that chemisorbed N forms $c(2 \times 2)$-reconstructed square islands with quite uniform size [83]. The fact that islands are formed indicates attractive interactions between chemisorbed N-atoms. The ideal island size is caused by an optimum between strain and edge energy. These islands exhibit long-range elastic interactions mediated by the substrate [84]. They repel each other at very long distances, they attract each other over intermediate distances, and they repel each other again at very short distances prohibiting island coalescence. The resulting scenario with increasing N-coverage is quite complex, but in brief it can be seen as follows. Once two islands approach each other into the attractive regime, they form a dimer to which further islands can only be added along its axis, whereas laterally approaching islands are repelled. This leads to island chains which can be compressed with increasing N coverage to a very regular lattice of quadratic N-covered islands separated by thin stripes of bare Cu, see Fig. 4(a) [48,83]. Since this lattice is stabilized by elastic relaxations in the substrate it is expected that the lattice constant of the N/Cu(100) template can be adjusted by working with

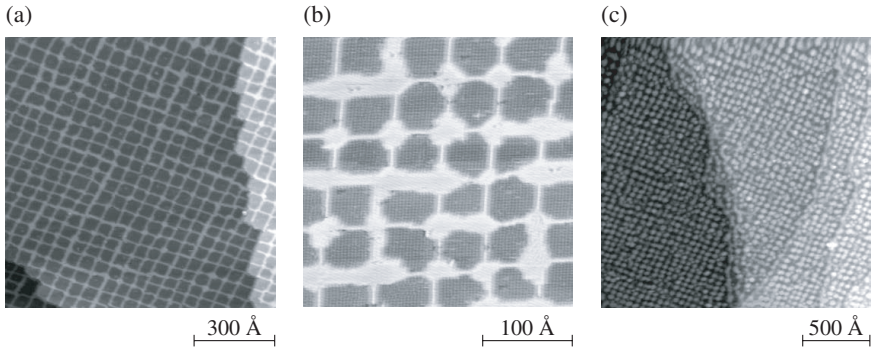

Fig. 4. (a) Quadratic areas of N-covered $c(2 \times 2)$-reconstructed Cu(100) form a regular lattice leaving only small stripes of bare Cu in-between ($\theta_N = 0.9$ ML of the $c(2 \times 2)$ structure, dosage of N_2 dissociated with filament, $T_{ads} = 630$ K). (b) STM image showing the $c(2 \times 2)$ structure atomically resolved ($\theta_N = 0.74$ ML of the $c(2 \times 2)$ structure). (c) Nucleation of Au islands at the intersection of the clean Cu stripes ($\theta_{Au} = 0.67$ ML, $T_{dep} = 300$ K, $\theta_N = 0.92$ ML of the $c(2 \times 2)$ structure). (a) from [85], (b) and (c) from [83].

Cu films of varying thickness on-top of a more rigid and lattice matched substrate.

Deposition of Au onto this surface leads to the nucleation of Au islands at the intersection of clean Cu stripes thus leading to a square island lattice with a period of 50 Å [83,86–88]. The N-covered Cu(100) surface has also been used for the growth of so far less well-ordered lattices of Fe and Cu [89], Co [90–92], Ag [93,94], and Ni [95]. We note that square lattices can in principle also be created on Au(14,15,15) since this miscut leads to 70 Å step distance, which is equal to the reconstruction period. However, the steps are already far apart reaching the limit of the elastic step repulsions which may render global order difficult. Finally we note that another interesting alternative square template, although with smaller lattice constant, is presented by the $(3\sqrt{3} \times 5)$-phase of V-oxide on Rh(111) [96].

5. Templates – Dislocation Networks and Ordered Domains in Biphases

Above we discussed surfaces which may serve as templates to grow square lattices. Here we present one more such example, however, with a larger lattice constant. Figure 5(a) shows the square lattice of misfit dislocations formed by 9 ML PbTe deposited onto PbSe(100) [97]. The system exhibits a

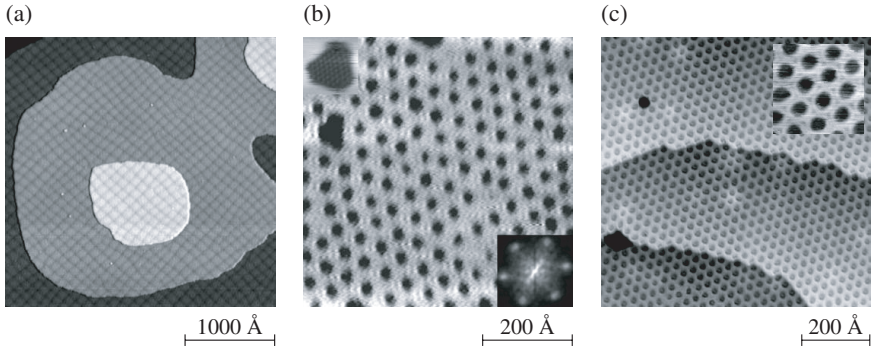

Fig. 5. (a) STM image of a regular square array of misfit dislocations for 9 ML of PbTe on PbSe(100) ($T_{\mathrm{growth}} = 380°\mathrm{C}$). (b) 2D crystal of Ag vacancy islands obtained by deposition of S onto 1 ML Ag on Ru(0001) ($\theta_{\mathrm{S}} = 0.10\,\mathrm{ML}$, $T = 300\,\mathrm{K}$). The inset shows that the vacancies are entirely covered by the chemisorbed sulfer. (c) STM image of a boron-nitride nanomesh formed by high-temperature decomposition of borazine on a Rh(111) surface (exposure 40 L $(\mathrm{HBNH})_3$ at 1070 K sample temperature, $V_{\mathrm{t}} = -1.0\,\mathrm{V}$ and $I_{\mathrm{t}} = 2.5\,\mathrm{nA}$, brighter spots are related to Ar bubbles in the near-surface region of the substrate). (a) from [97], (b) from [98], and (c) from [99].

high dislocation mobility since the dislocation glide plane is parallel to the surface; in addition, the dislocations nucleate in a homogeneous way, and finally they strongly repel each other. These factors lead to the well-ordered superlattice with a lattice constant of 101 ± 12 Å.

Domain patterns evolving from the spinodial decomposition of two surface phases are often very well-ordered due to long-range repulsive dipolar elastic interactions. One example is N/Cu(100) discussed above, where the two phases are the $c(2 \times 2)$-structured islands of chemisorbed N, and the clean Cu(100) surface. For close-packed surfaces one observes, with increasing coverage of one phase at the dispense of the other, a transition from droplets to stripes to inverse droplets, as reported for the Ag/Pt(111) surface alloy [100], and for a Pb overlayer coexisting with a PbCu alloy-phase on Cu(111) [101]. Here we focus on another example where S is adsorbed onto a Ag covered Ru(0001) surface [98]. S binds strongly to the Ru substrate and therefore displaces Ag, by which it compresses the Ag layer. This leads to a hexagonal lattice of islands of chemisorbed S which repel each other by the compressive stress in the Ag layer, see Fig. 5(b). The islands are 24 ± 4 Å in diameter and the lattice parameter is 53 Å.

The last example we would like to discuss is a lattice of holes formed in stoichiometric hexagonal (*h*) BN double layers on Rh(111), see Fig. 5(c) and [99]. The lattice is composed of holes in the BN-bilayer with a diameter of 24 ± 2 Å, and an average distance of 32 ± 2 Å. The holes in the upper layer are offset with respect to the smaller holes in the lower layer. We note that well-ordered superstructures with a large period have already been observed some time ago by means of LEED for borazine adsorption onto Re(0001) [102], while borazine adsorption onto other close-packed metal surfaces, such as Pt(111), Pd(111), and Ni(111), leads to the self-limiting growth of commensurate *h*-BN monolayers [103,104]. For BN/Rh(111) it is not clear at present whether the Rh(111) substrate is exposed at the bottom of the holes. If this was the case the surface would not only be periodic in morphology but also in chemistry, and therefore would constitute a very useful template for the growth of ordered superlattices of metals, semiconductors, and molecules.

6. Outlook

We were discussing various ways to create ordered superlattices of atoms, molecules, and islands. Atomic superlattices are monodisperse and can be

stabilized by electronic screening in a 2D electron gas. Also, metal islands on Si(111)-(7 × 7) are monodisperse. In these systems the metal atoms form strong bonds with Si surface atoms creating M_xSi_y-silicide clusters with preferred size, see the example of Al_6Si_3 presented in [78–80]. The islands created by heterogeneous nucleation on periodic surfaces and the vertically stacked QDs are not monodisperse, however, they can potentially reach size distributions down to a few % in width. All superlattices are metastable structures created by the diffusion of adspecies on long-range modulated potential energy surfaces. The stability is lowest for the atomic superlattices which, upon annealing, first nucleate small islands which then Ostwald ripen to larger islands [105,106] until eventually these islands also decay to form a seam at the substrate steps. Adsorbates forming alloys with the substrate may even disappear into the bulk upon annealing.

The examples given here concern atoms and islands, and in most cases were not yet extended to molecules, which will be very interesting to explore. Many of the templates presented here have not yet been used for the creation of superlattices. It will be interesting to investigate how, for example, the BN-lattice will behave when depositing metals, semiconductors, or molecules on top (C_{60} molecules have already been adsorbed [99]). For larger distances the PbTe/PbSe(100) dislocation network will be a good candidate, and for small distances, for example of catalytic particles, the reconstructions of bulk oxide surfaces and the ones of thin epitaxial oxide-films are promising templates. Following the approaches used in 3D supramolecular chemistry, one has realized 2D molecular superlattices with cavities exposing the underlying metal substrate [107–111]. These lattices may in the future also be employed as templates for metal or semiconductor deposition. Future work into this direction will have to address the stability of the molecular lattice towards the highly reactive diffusing adsorbates, and the challenge of obtaining a filling factor of 1 for the molecular superlattices, since up to now in many cases only half of the surface is covered with the superlattices. Regular lattices of 1D stripes may also be achieved with molecules [112], and recently it was shown that a striped biphase surface can be used as template for molecular decoration [113].

We hope that the present overview inspires future work in the creation of well-defined atomic, molecular and island superlattices at surfaces, opening up the investigation of the novel properties also with spatially integrating experimental techniques.

Acknowledgments

The author would like to acknowledge fruitful discussions with G. Springholz, T. Greber, W. D. Schneider, J. V. Barth, V. S. Stepanyuk, and P. Bruno.

References

[1] P. Gambardella, S. Rusponi, M. Veronese, S. S. Dhesi, C. Grazioli, A. Dallmeyer, I. Cabria, R. Zeller, P. H. Dederichs, K. Kern, C. Carbone and H. Brune, *Science* **300**, 1130–1133 (2003).
[2] F. Silly, M. Pivetta, M. Ternes, F. Patthey, J. P. Pelz and W. D. Schneider, *Phys. Rev. Lett.* **92**, 016101 (2004).
[3] M. Ternes, C. Weber, M. Pivetta, F. Patthey, J. P. Pelz, T. Giamarchi, F. Mila and W. D. Schneider, *Phys. Rev. Lett.* **93**, 146805 (2004).
[4] R. W. Chantrell, N. Walmsley, J. Gore and M. Maylin, *Phys. Rev. B* **63**, 024410 (2001).
[5] M. C. Bartelt, M. C. Tringides and J. W. Evans, *Phys. Rev. B* **47**, 13891 (1993).
[6] J. G. Amar and F. Family, *Phys. Rev. Lett.* **74**, 2066 (1995).
[7] M. C. Bartelt and J. W. Evans, *Phys. Rev. B* **54**, R17359 (1996).
[8] P. A. Mulheran and J. A. Blackman, *Phys. Rev. B* **53**, 10261 (1996).
[9] H. Brune, *Surf. Sci. Rep.* **31**, 121 (1998).
[10] J. Friedel, *Nuovo Cimento Suppl.* **7**, 287–311 (1958).
[11] K. H. Lau and W. Kohn, *Surf. Sci.* **75**, 69–85 (1978).
[12] T. L. Einstein, *Surf. Sci.* **75**, 161L (1978).
[13] T. L. Einstein, Interactions between adsorbed particles, in *Handbook of Surface Science*, Vol. 1, ed. W. N. Unertl (Elsevier Science B. V., New York, 1996), p. 578.
[14] K. H. Lau and W. Kohn, *Surf. Sci.* **65**, 607–618 (1977).
[15] E. Wahlström, I. Ekvall, H. Olin and L. Walldén, *Appl. Phys. A* **66**, S1107–S1110 (1998).
[16] J. Repp, F. Moresco, G. Meyer, K. H. Rieder, P. Hyldgaard and M. Persson, *Phys. Rev. Lett.* **85**, 2981 (2000).
[17] N. Knorr, H. Brune, M. Epple, A. Hirstein, A. M. Schneider and K. Kern, *Phys. Rev. B* **65**, 115420 (2002).
[18] H. Brune, J. Wintterlin, G. Ertl and R. J. Behm, *Europhys. Lett.* **13**, 123–128 (1990).
[19] O. Jeandupeux, L. Bürgi, A. Hirstein, H. Brune and K. Kern, *Phys. Rev. B* **59**, 15926–15934 (1999).
[20] N. W. Ashcroft and N. D. Mermin, *Solid State Physics* (HRW, Philadelphia, 1987).
[21] M. F. Crommie, C. P. Lutz and D. M. Eigler, *Nature* **363**, 524–527 (1993).
[22] J. A. Venables and H. Brune, *Phys. Rev. B* **66**, 195404 (2002).

[23] G. Ehrlich and F. Watanabe, *Langmuir* **7**, 2555–2563 (1991).
[24] S. J. Stranick, M. M. Kamna and P. S. Weiss, *Science* **266**, 99 (1994).
[25] J. Trost, T. Zambelli, J. Wintterlin and G. Ertl, *Phys. Rev. B* **54**, 17850–17857 (1996).
[26] P. Hyldgaard and M. Persson, *J. Phys.-Condens. Mat.* **12**, L13–L19 (2000).
[27] N. Knorr, M. A. Schneider, C. F. J. Flipse, L. Vitali, L. Diekhöner, P. Wahl, H. Brune and K. Kern, *unpublished* (2005).
[28] S. J. Koh and G. Ehrlich, *Phys. Rev. Lett.* **87**, 106103 (2001).
[29] K. A. Fichthorn, M. L. Merrick and M. Scheffler, *Phys. Rev. B* **68**, 041404 (2003).
[30] V. S. Stepanyuk, A. N. Baranov, D. V. Tsivlin, W. Hergert, P. Bruno, N. Knorr, M. A. Schneider and K. Kern, *Phys. Rev. B* **68**, 205410 (2003).
[31] V. S. Stepanyuk, L. Niebergall, R. C. Longo, W. Hergert and P. Bruno, *Phys. Rev. B* **70**, 075414 (2004).
[32] K. A. Fichthorn, M. L. Merrick and M. Scheffler, *Appl. Phys. A* **75**, 17 (2002).
[33] C. Liu, S. Yamazaki, R. Hobara, I. Matsuda and S. Hasegawa, *Phys. Rev. B* **71**, 041310 (2005).
[34] R. Leon, Y. Kim, C. Jagedish, M. Gal, J. Zuo and D. J. H. Cockayne, *Appl. Phys. Lett.* **69**, 1888 (1996).
[35] D. Leonard, M. Krishnamurthy, C. M. Reaves, S. P. Denbaars and P. M. Petroff, *Appl. Phys. Lett.* **63**, 3203 (1993).
[36] J. M. Moison, F. Houzay, F. Barthe, L. Leprince, E. André and O. Vatel, *Appl. Phys. Lett.* **64**, 196 (1994).
[37] J. Tersoff, C. Teichert and M. G. Lagally, *Phys. Rev. Lett.* **76**, 1675 (1996).
[38] G. Springholz, V. Holy, M. Pinczolits and G. Bauer, *Science* **282**, 734–737 (1998).
[39] P. A. Mulheran and J. A. Blackman, *Phil. Mag. Lett.* **72**, 55 (1995).
[40] J. Tersoff and F. K. LeGoues, *Phys. Rev. Lett.* **72**, 3570–3573 (1994).
[41] C. Teichert, M. G. Lagally, L. J. Peticolas, J. C. Bean and J. Tersoff, *Phys. Rev. B* **53**, 16334 (1996).
[42] Q. H. Xie, A. Madhukar, P. Chen and N. P. Kobayashi, *Phys. Rev. Lett.* **75**, 2524 (1995).
[43] G. S. Solomon, J. A. Trezza, A. F. Marshall and J. S. Harris, *Phys. Rev. Lett.* **76**, 952 (1996).
[44] F. Liu, S. E. Davenport, H. M. Evans and M. G. Lagally, *Phys. Rev. Lett.* **82**, 2528 (1999).
[45] M. Pinczolitis, G. Springholz and G. Bauer, *Phys. Rev. B* **60**, 11524 (1999).
[46] G. Springholz, M. Pinczolits, P. Mayer, V. Holy, G. Bauer, H. H. Kang and L. Salamanca-Riba, *Phys. Rev. Lett.* **84**, 4669 (2000).
[47] J. V. Barth, H. Brune, G. Ertl and R. J. Behm, *Phys. Rev. B* **42**, 9307 (1990).
[48] S. Rousset, V. Repain, G. Baudot, H. Ellmer, Y. Garreau, V. Etgens, J. M. Berroir, B. Croset, M. Sotto, P. Zeppenfeld, J. Ferré, J. P. Jamet, C. Chappert and J. Lecoeur, *Mat. Sci. Eng. B* **96**, 169–177 (2002).

[49] V. Repain, J. M. Berroir, B. Croset, S. Rousset, Y. Garreau, V. H. Etgens and J. Lecoeur, *Phys. Rev. Lett.* **84**, 5367 (2000).
[50] R. J. Hamers, R. M. Tromp and J. E. Demuth, *Phys. Rev. Lett.* **56**, 1972 (1986).
[51] N. G. Condon, F. M. Leibsle, T. Parker, A. R. Lennie, D. J. Vaughan and G. Thornton, *Phys. Rev. B* **55**, 15885–15894 (1997).
[52] H. Brune, H. Röder, C. Boragno and K. Kern, *Phys. Rev. B* **49** (1994) 2997.
[53] C. Günther, J. Vrijmoeth, R. Q. Hwang and R. J. Behm, *Phys. Rev. Lett.* **74**, 754 (1995).
[54] H. Brune and K. Kern, Heteroepitaxial metal growth: The effects of strain, in *Growth and Properties of Ultrathin Epitaxial Layers*, Vol. 8 of *The Chemical Physics of Solid Surfaces and Heterogeneous Catalysis*, eds. D. A. King and D. P. Woodruff (Elsevier Science, Amsterdam, 1997), p. 149.
[55] W. L. Ling, J. de la Figuera, N. C. Bartelt, R. Q. Hwang, A. K. Schmid, G. E. Thayer and J. C. Hamilton, *Phys. Rev. Lett.* **92**, 116102 (2004).
[56] R. M. Jaeger, H. Kuhlenbeck, H. J. Freund, M. Wuttig, W. Hoffmann, R. Franchy and H. Ibach, *Surf. Sci.* **259**, 235 (1991).
[57] H. C. Galloway, J. J. Benítez and M. Salmeron, *Surf. Sci.* **298**, 127 (1993).
[58] T. Wiederholt, H. Brune, J. Wintterlin, R. J. Behm and G. Ertl, *Surf. Sci.* **324**, 91 (1995).
[59] A. Rosenhahn, J. Schneider, C. Becker and K. Wandelt, *J. Vac. Sci. Tech. A* **18**, 1923 (2000).
[60] S. A. Chambers. *Surf. Sci. Rep.* **39**, 105 (2000).
[61] T. Maroutian, S. Degen, C. Becker, K. Wandelt and R. Berndt, *Phys. Rev. B* **68**, 155414 (2003).
[62] J. Schoiswohl, M. Sock, S. Eck, S. Surnev, M. G. Ramsey, F. P. Netzer and G. Kresse, *Phys. Rev. B* **69**, 155403 (2004).
[63] M. Horn-von Hoegen, A. Al. Falou, H. Pietsch, B. H. Müller and M. Henzler, *Surf. Sci.* **298**, 29 (1993).
[64] M. Böhringer, P. Molinàs-Mata, E. Artacho and J. Zegenhagen, *Phys. Rev. B* **51**, 9965 (1995).
[65] M. Böhringer, Q. Jiang, R. Berndt, W. D. Schneider and J. Zegenhagen, *Surf. Sci.* **367**, 245 (1996).
[66] J. de la Figuera, K. Pohl, A. K. Schmid, N. C. Bartelt, J. Hrbek and R. Q. Hwang, *Surf. Sci.* **433–435**, 93–98 (1999).
[67] F. Besenbacher, L. Pleth Nielsen and P. T. Sprunger, Surface alloying in heteroepitaxial metal-on-metal growth, in *Growth and Properties of Ultrathin Epitaxial Layers*, Vol. 8 of *The Chemical Physics of Solid Surfaces and Heterogeneous Catalysis*, eds. D. A. King and D. P. Woodruff (Elsevier Science, Amsterdam, 1997), p. 207.
[68] H. Brune, M. Giovannini, K. Bromann and K. Kern, *Nature* **394**, 451–453 (1998).
[69] M. Böhringer, K. Morgenstern, W. D. Schneider, R. Berndt, F. Mauri, A. De Vita and R. Car, *Phys. Rev. Lett.* **83**, 324 (1999).

[70] T. Yokoyama, S. Yokoyama, T. Kamikado, Y. Okuno and S. Mashiko, *Nature* **413**, 619–621 (2001).
[71] V. Repain, G. Baudot, H. Ellmer and S. Rousset, *Europhys. Lett.* **58**, 730–736 (2002).
[72] S. Rohart, G. Baudot, V. Repain, Y. Girard, S. Rousset, H. Bulou, C. Goyhenex and L. Proville, *Surf. Sci.* **559**, 47–62 (2004).
[73] C. Becker, A. Rosenhahn, A. Wiltner, K. von Bergmann, J. Schneider, P. Pervan, M. Milun, M. Kralj and K. Wandelt, *N. J. Phys.* **4**, 75 (2002).
[74] S. Degen, C. Becker and K. Wandelt, *Faraday Discuss.* **125**, 343–356 (2004).
[75] L. Vitali, M. G. Ramsey and F. P. Netzer, *Phys. Rev. Lett.* **83**, 316 (1999).
[76] M. Y. Lai and Y. L. Wang, *Phys. Rev. B* **64**, 241404 (2001).
[77] J. L. Li, J. F. Jia, X. J. Liang, X. Liu, J. Z. Wang, Q. K. Xue, Z. Q. Li, J. S. Tse, Z. Zhang and S. B. Zhang, *Phys. Rev. Lett.* **88**, 066101 (2002).
[78] J. Jia, J.-Z. Wang, X. Liu, Q.-K. Xue, Z.-Q. Li, Y. Kawazoe and S. B. Zhang, *Appl. Phys. Lett.* **80**, 3186 (2002).
[79] V. G. Kotlyar, A. V. Zotov, A. A. Saranin, T. V. Kasyanova, M. A. Cherevik, I. V. Pisarenko and V. G. Lifshits, *Phys. Rev. B* **66**, 165401 (2002).
[80] J.-F. Jia, X. Liu, J.-Z. Wang, J.-L. Li, X. S. Wang, Q.-K. Xue, Z.-Q. Li, Z. Zhang and S. B. Zhang, *Phys. Rev. B* **66**, 165412–165421 (2002).
[81] K. Wu, Y. Fujikawa, T. Nagao, Y. Hasegawa, K. S. Nakayama, Q. K. Xue, E. G. Wang, T. Briere, V. Kumar, Y. Kawazoe, S. B. Zhang and T. Sakurai, *Phys. Rev. Lett.* **91**, 126101 (2003).
[82] H. H. Chang, M. Y. Lai, J. W. Wei, C. M. Wei and Y. L. Wang, *Phys. Rev. Lett.* **92**, 066103 (2004).
[83] H. Ellmer, V. Repain, M. Sotto and S. Rousset, *Surf. Sci.* **511**, 183 (2002).
[84] B. Croset, Y. Girard, G. Prévot, M. Sotto, Y. Garreau, R. Pinchaux and M. Sauvage-Simkin, *Phys. Rev. Lett.* **88**, 56103 (2002).
[85] S. Rousset, B. Croset, Y. Girard, G. Prévot, V. Repain and S. Rohart, *C. R. Physique* **6**, 33–46 (2005).
[86] F. Leibsle, S. S. Dhesi, S. Barrett and A. Robinson, *Surf. Sci.* **317**, 309 (1994) .
[87] M. Sotto and B. Croset, *Surf. Sci.* **461**, 78 (2000).
[88] H. Ellmer, V. Repain, S. Rousset, B. Croset, M. Sotto and P. Zeppenfeld, *Surf. Sci.* **476**, 95 (2001).
[89] T. M. Parker, L. K. Wilson, N. G. Condon and F. M. Leibsle, *Phys. Rev. B* **56**, 6458 (1997).
[90] S. L. Silva, C. R. Jenkins, S. M. York and F. M. Leibsle, *Appl. Phys. Lett.* **76**, 1128–1130 (2000).
[91] K. Mukai, Y. Matsumoto, K. Tanaka and F. Komori, *Surf. Sci.* **450**, 44 (2000).
[92] F. Komori, K. Lee, K. Nakatsuji, T. Imori and Y. Cai, *Phys. Rev. B* **63**, 214420 (2001).
[93] S. L. Silva and F. M. Leibsle, *Surf. Sci.* **440**, L835 (1999).
[94] F. Leibsle, *Surf. Sci.* **514**, 33–40 (2002).
[95] Y. Matsumoto and K. Tanaka, *Jap. J. Appl. Phys.* **37**, L154 (1998).

[96] J. Schoiswohl, G. Kresse, S. Surnev, M. Sock, M. G. Ramsey and F. P. Netzer, *Phys. Rev. Lett.* **92**, 206103 (2004).
[97] G. Springholz and K. Wiesauer, *Phys. Rev. Lett.* **88**, 15507 (2002).
[98] K. Pohl, M. C. Bartelt, J. de la Figuera, N. C. Bartelt, J. Hrbek and R. Q. Hwang, *Nature* **397**, 238 (1999).
[99] M. Corso, W. Auwärter, M. Muntwiler, A. Tamai, T. Greber and J. Osterwalder, *Science* **303**, 217–220 (2004).
[100] H. Röder, R. Schuster, H. Brune and K. Kern, *Phys. Rev. Lett.* **71**, 2086 (1993).
[101] R. Plass, J. A. Last, N. C. Bartelt and G. L. Kellogg, *Nature* **412**, 875 (2001).
[102] J. W. He and D. W. Goodman, *Surf. Sci.* **232**, 138–148 (1990).
[103] A. Nagashima, N. Tejima, Y. Gamou, T. Kawai and C. Oshima, *Surf. Sci.* **357–358**, 307 (1996).
[104] W. Auwärter, T. J. Kreutz, T. Greber and J. Osterwalder, *Surf. Sci.* **429**, 229 (1999).
[105] H. Röder, E. Hahn, H. Brune, J. P. Bucher and K. Kern, *Nature* **366**, 141 (1993).
[106] H. Brune, G. S. Bales, C. Boragno, J. Jacobsen and K. Kern, *Phys. Rev. B* **60**, 5991 (1999).
[107] A. Dmitriev, N. Lin, J. Weckesser, J. V. Barth and K. Kern, *J. Phys. Chem. B* **106**, 6907 (2002).
[108] J. A. Theobald, N. S. Oxtoby, M. A. Phillips, N. R. Champness and P. H. Beton, *Nature* **424**, 1029–1031 (2003).
[109] A. Dmitriev, H. Spillmann, N. Lin, J. V. Barth and K. Kern, *Angew. Chem. Int. Ed.* **42**, 2670 (2003).
[110] H. Spillmann, A. Dmitriev, N. Lin, P. Messina, J. V. Barth and K. Kern, *J. Am. Chem. Soc.* **125**, 10725 (2003).
[111] S. Stepanow, M. Lingenfelder, A. Dmitriev, H. Spillmann, E. Delvigne, N. Lin, X. Deng, C. Cai, J. V. Barth and K. Kern, *Nat. Mater.* **3**, 229–233 (2004).
[112] J. V. Barth, J. Weckesser, G. Trimarchi, M. Vladimirova, A. De Vita, C. Cai, H. Brune, P. Günter and K. Kern, *J. Am. Chem. Soc.* **124**, 7991–8000 (2002).
[113] R. Otero, Y. Naitoh, F. Rosei, P. Jiang, P. Thostrup, A. Gourdon, E. Lgsgaard, I. Stensgaard, C. Joachim and F. Besenbacher, *Angew. Chem. Int. Ed.* **43**, 2091–2095 (2004).